

Chapter 2

Materials and Experimental Details

Abstract

In this chapter, thermoplastic polymers, experimental technique and various characterisation techniques (to do off-line analysis of the pristine and plasma treated samples) used are discussed. The working principles of these techniques are explained briefly.

2.1 Polymers Studied

2.1.0 Introduction

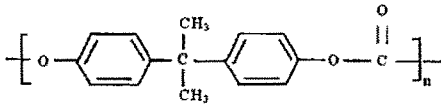
Surface modification of thermoplastic polymers, experimental procedures, and the characterization techniques used in the analysis of plasma polymers interaction are presented in this chapter. The plasma chamber used is described in detail as the main set up during the sample treatment. To investigate the interaction / basic chemical properties of plasma polymers, X-ray Photoelectron Spectroscopy (XPS), Attenuated total reflection Fourier transform infrared (ATR-FTIR) spectroscopy, Contact Angle Goniometry and Atomic Force Microscopy (AFM) are introduced. Hardness measurements have been used to investigate the materials response to plasma irradiation since elastic properties and hardness are related to crosslink number density [91] and can be measured accurately and conveniently [92, 93].

The details of thermoplastic polymers used in this study are discussed in following sub-sections.

2.1.1 Polycarbonate (PC)

Polycarbonate is a thermoplastic polymer. Polycarbonate is becoming more common in housewares as well as laboratories and in industry, especially in applications where any of its main features—high impact resistance, temperature resistance, optical properties—are required. It is also known as bisphenol-A polycarbonate. It is a clear material having a slight yellowish discoloration. Polycarbonates have good resistance to water, dilute acids, oxidising and reducing agents, hydrocarbons, and other chemicals at room temperature. Electrical properties are good, and are not adversely affected over a range of temperatures and humidity. Section 1.7 (Chapter-1) describes the motivation of selecting PC as a thermoplastic polymer for present study.

Polymeric materials have been able to replace traditional engineering materials like metals and glass because of their high strength to weight ratio, resistance to corrosion, possibility of recycling and their relatively low cost. Its chemical structure is mentioned as



Typical Applications:

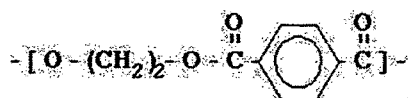
- Drinking bottles and glasses
- Lighting lenses, sunglass/eye glass lenses, safety glasses, automotive head lamp lenses
- Compact discs, DVDs, MP3/Digital audio player cases
- Toys (like spinning tops/RC Cars.etc)
- Advertisement: signs, displays, poster protection
- Building: domelights, flat or curved glazing
- Computers: laptops and computer cases
- Industry: lab equipment enclosures, instrument panels
- Hobby: Machined into fins, gyro mounts, and flybar locks for use with radio-controlled helicopters

2.1.2 Polyethylene terephthalate (PET)

Polyethylene terephthalate (PET) is a condensation polymer produced from the monomers ethylene glycol, $\text{HOCH}_2\text{CH}_2\text{OH}$, a dialcohol, and dimethyl terephthalate, $\text{CH}_3\text{O}_2\text{C}-\text{C}_6\text{H}_4-\text{CO}_2\text{CH}_3$, a diester. By the process of transesterification, these monomers form ester linkages between them, yielding a polyester. These polymers

often called polyester. Section 1.7 (Chapter-1) describes the motivation of selecting commercial grade PET as a thermoplastic polymer for present study.

Surface modifications in general and especially the metallization of polyethylene terephthalate (PET) have been of great importance ever since they have been widely applied in a number of fields such as packaging, decorative coatings, capacitors, magnetic tape, eyeglass lenses etc. PET is one of the most important thermoplastic used in the microelectronics; biomedical field because of its excellent mechanical properties due to the presence of the aromatic ring in polymer structure. PET is a colorless semi-crystalline resin. The chemical structure of PET is mentioned as



Typical Applications:

- PET is a excellent barrier material used in plastic bottles for soft drinks.
- Food packaging and thermal insulation
- Used as substrate in thin film and solar cell

2.1.3 Polytetrafluoroethylene (PTFE)

PTFE is a unique class of polymers, which have since found use in everything from missiles to frying pans. PTFE is a carbon backbone polymer that is readily synthesized by emulsion polymerization of tetrafluoroethylene, forming repeating linear chains of $(-\text{CH}_2-\text{CH}_2-)_n$ which is illustrated in **Figure 2.1**. This atomic arrangement conforms to a helical carbon backbone with dihedral angle between 160° and 165° , forming a complete sheath of fluorine atoms around the carbon backbone. High fluorination of the carbon backbone decreases the amount of unfulfilled bonds, leading to a polymer with low intrinsic surface tension of 22.5 mN/m. [94] PTFE covalent bond energies are

among the strongest in single bond organic chemistry, with C-F bond energies of 481 kJ/mol (4.99 eV/atom) and C-C bond energies of 348 kJ/mol (3.61 eV/atom), making them harder to dissociate as compared to other single bond polymers [94]. The steric effects of the fluorine atoms perfectly balance the charges across the polymer chain cross section and are therefore non-polar. High bond energies, non-polar structural arrangement, and tight intermolecular packing are responsible for PTFE's chemical inertness.

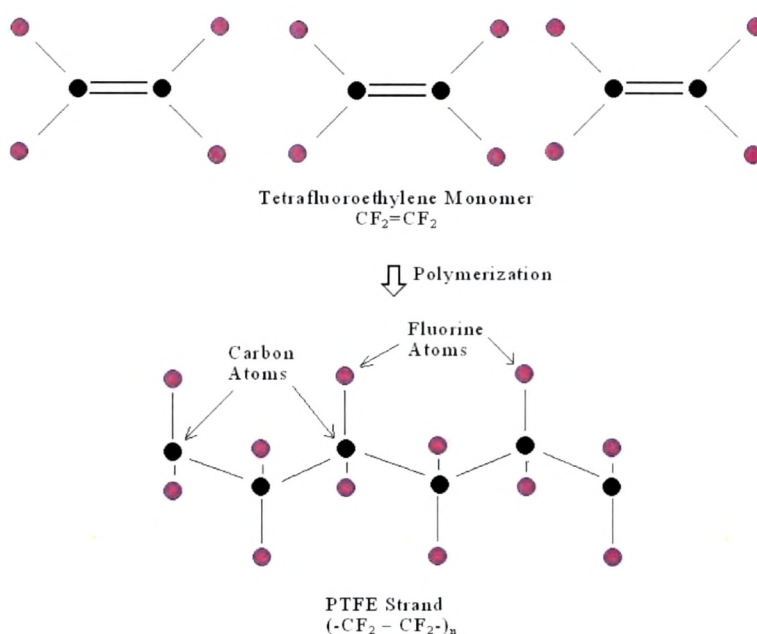


Figure 2.1: Illustration of polymerization of tetrafluoroethylene into PTFE

The tightly packed polymer morphology facilitates chain alignment, allowing high polymer crystallinities of 70-90%. Bond forces between two adjacent polymer chains are significantly lower than the forces within one chain, which are typically 3 kJ/mol. This low molecular cohesion is partially responsible for a coefficient of friction of 0.1, the lowest of any material; however, it also facilitates mechanical creep due to chain movement. The unbranched morphology and low interpolymer chain attraction requires

very long chain lengths, increasing the melting point of PTFE to nearly 300 °C. Section 1.7 (Chapter-1) describes the motivation of selecting a PTFE thermoplastic polymer for present study.

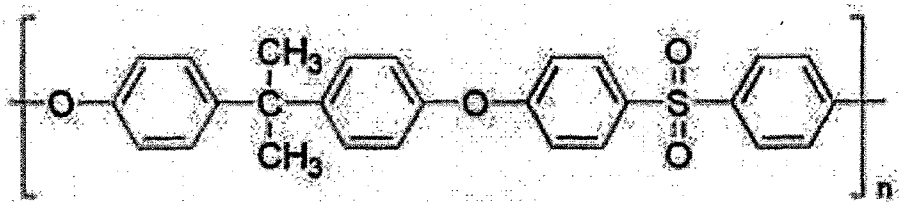
Typical Applications:

- Polytetrafluoroethylene (PTFE) is a polymer used as insulator in cables, connector assemblies and for printed circuit boards because of its good dielectric properties [91].
- In medical products and surgical instruments, polymeric devices are improving current healthcare practice. The polymeric devices are meeting the requirements of biocompatibility between the physiological environment and the biomaterial surface. Mostly PTFE is used as vascular grafts in cardiovascular applications. In many applications where good adhesion between a polymer and a coating is necessary, it must be modified to assure better adhesiveness.

2.1.4 Polyethersulfone (PES)

Polyethersulfone (PES) is a heat resistant, transparent, amber, non-crystalline thermoplastic polymer. PES is tough and rigid polymer similar to polycarbonate. As it can stand up well to water and steam, PES is used to make cookware and medical products that need to be sterilized between uses. PES get their name because they have ether groups and sulfone groups in their backbone chains. Section 1.7 (Chapter-1) describes the motivation of selecting PES as a thermoplastic polymer for present study.

The chemical structure of PES is mentioned as



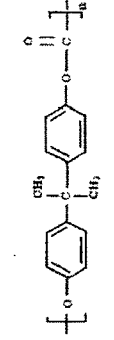
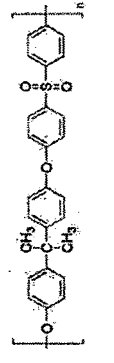


Typical Applications:

- PES has the highest service temperature
- PES membranes can be used in hemodialysis, waste water recovery, gas separation and food and beverages processing.
- PES are also used in automotive and electronics industries
- It is used as a dielectric in capacitors
- It is used as filtration media

The physical and chemical properties of all polymers used in the present work are listed in **Table 2.1**.

Table 2.1: Some of the physical and chemical properties of the polymers used [95]

Property	PTFE	PET	PC	PES
Molecular Formula	$(C_2F_4)_n$	$(C_{10}H_8O_4)_n$	$----[-C_{16}H_{14}O_3-]_n----$	$----[C_{27}H_{22}O_4S]_n----$
Chemical structure				
Polymer type	Thermoplastic polymer	Thermoplastic polymer	Thermoplastic polymer	Thermoplastic polymer
Density (g/cm ³) at 25°C	2.2	1.4	1.2 – 1.22	1.43
Molecular weight	100.02 g/mol	192.2 g/mol	254.3 g/mol	232.26 g/mole
Refractive index	1.38	1.57	1.584 – 6	1.65
Dielectric constant @ 1 MHz	160 kV/mm	3	2.9	3.7
Dissipation factor @ 1 MHz	<0.0001	0.016	0.01	0.003
Heat deflection temperature	120°C	115°C	140 °C	>260°C
Melting temperature	327°C	250°C	267 °C	340 – 428 °F
Glass transition temperature	27°C	76°C	150 °C	185°C

2.2 Details of plasma treatment

Plasma treatment can modify the surface of a polymer substrate by physical and chemical changes. The plasma capable of exerting four major effects, that is, contamination removal, surface activation, etching and cross-linking [Chapter 1, Section 1.4 (iii)] with concomitant effects on wetting, coloration, surface adhesion, electrical conductivity and other characteristics of interest in industry. Depending on the plasma parameters, one of these changes can predominate on the others.

Instrument consists of vacuum chamber, manifold unit, vacuum pump, power distribution box, and bipolar pulsed power supply. Actual plasma process takes place in the vacuum chamber which consists of an aluminum container. Experiments were performed with PC, PET, PTFE and PES films, which were cut to small pieces of about 2.0 cm × 2.0 cm size. All samples were cleaned in isopropyl alcohol and dried before inserting into the plasma chamber. The set up consists of 60 cm long cylindrical chamber of 30 cm diameter. It has two rectangular parallel plates of stainless steel of dimensions 16 cm x 7.5 cm, which works as electrodes. The inter electrode gap was maintained 2 cm in all the experiments. The Schematic of the experimental setup is shown in **Figure 2.2**. Bipolar pulsed power source was used to generate the desired argon plasma. [46] The applied Voltage and current were measured with the help of high voltage probe (Tektronix P6015A, 1000X) and current transformer respectively. Tektronix (TDS 2024, 200MHz) digital oscilloscope was used to record the voltage and current waveforms (**Figure 2.3**). The chamber pressure was 0.1 mbar during the argon plasma treatment. The samples were treated in argon plasma for 5, 10 and 50 minutes respectively. When the treatment time was

over, the reactor was kept under oxygen atmosphere for 30 more minutes, to enhance remaining surface active radicals to react with oxygen. This also protected the surface against contamination that could have occurred when the reactor was opened to air.

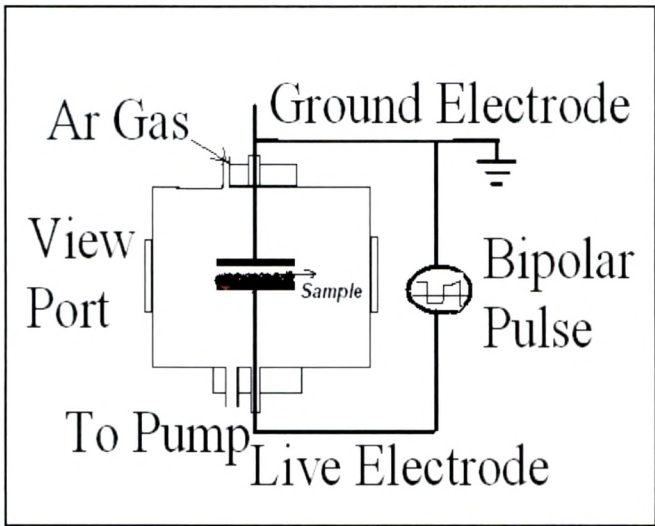


Figure 2.2: Schematic of the experimental set-up

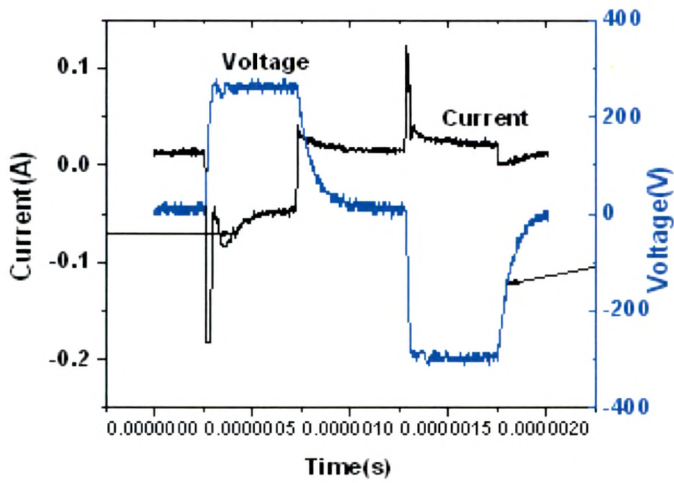


Figure 2.3: Voltage and current waveform

2.3 Characterization techniques

2.3.0 Introduction

A large number of techniques are available for the analysis of polymer surfaces having its own advantages and disadvantages. The suitability of a particular technique depends upon the specific problem under examination. It is highly desirable to examine the same sample by different techniques. Different techniques offer cross data and assists in interpretation. Various types of information may be obtained such as optical, chemical, and structural properties. In the present study, chemical composition was obtained from x-ray photoelectron spectroscopy (XPS) while surface energetic was evaluated from contact angle goniometry. ATR-FTIR spectroscopy was used to cross check the information received from XPS. AFM will provide topographical information. Microhardness testing was performed to measure the resistance to plastic deformation. Different characterization techniques with their working principle and specifications have been discussed in the following subsections.

2.3.1 Contact angle goniometry

Contact angle measurement is the most commonly used method of solid surface tension measurement. Contact angle is determined by the outermost atomic layers of a surface (0.1-1 nm). The surface atoms and molecules are in different environment as compared to their bulk counterparts. In the bulk, a molecule is attracted equally in all directions by its neighbouring molecules, while the surface molecules are subjected to intermolecular attraction from one side only. At the equilibrium state, the lower density in the surface layer increased the intermolecular distance, putting it in a state of tension.



Figure 2.4: *Contact angle goniometer (NRL C.A. Goniometer, Model 100-00-230)*

The contact angles were measured with a contact angle goniometer (NRL C.A. Goniometer, Model 100-00-230) as shown in **Figure 2.4**. During contact angle measurements, a drop of liquid (5 μl) was placed onto the treated polymer surface by a microsyringe. For the calculation of the contact angles, the tangent leaning method was used for all measurements. At equilibrium, the angle was measured by a camera equipped with a goniometric eyepiece. Each value of contact angle was taken as an average value of five different points on the same sample surface. Surface free energy, sum of polar and dispersion components was calculated by measuring contact angle with two different liquids (water and glycerin) on polymer surfaces.

Contact angle measurements are affected by various factors, like surface preparation, contamination, environment, temperature, and drop size. Inhomogeneous solid surfaces created by roughness, or contamination, or the sample preparation method can give different contact angle values for the same material. The effect of the environment on contact angle is usually caused by the adsorption of vapour onto a polymer surface reducing the tension of the polymer

surface, and again giving different results in different environmental conditions. It is also important to pay attention to the experimental temperature and the drop size. The increase in the values of these two parameters will result in a decrease in the contact angle.

(a) Wettability

Wetting a solid surface by a liquid is a surface phenomenon in which liquid spreads on the surface and tends to cover it. Depending of chemical activities, wetting of solid surfaces can be classified into nonreactive and reactive wetting. The wetting in which liquid spreads on a substrate without chemical reaction or absorption is called nonreactive wetting, and if it is influenced by chemical reactions between spreading liquid and substrate material is called reactive wetting. Depending on how the process is initiated, the wetting is further classified into spontaneous spreading and driven spreading. In spontaneous spreading, the liquid spreads on a solid by itself without external interference and driven spreading is initiated (driven) by some kind of external actions. In our experiments, we incorporated nonreactive spontaneous wetting.

When a drop of liquid is put in contact with a flat polymer surface, the tri-phase boundary that separates the three phases (solid state, liquid state and vapour state) is known as contact line. If the substrate is chemical homogeneous and uniform, the contact line is a circle. The plane containing the normal of the solid surface and cutting through the apex of the liquid droplet is known as the meridian plane. The angle between the solid surface and the tangent of the liquid at the tri-phase contact point in the meridian plane through the liquid phase is called contact angle.

The phenomenon of existence of multiple contact angles for the same test liquid is known as hysteresis. Among all observed contact angles for liquid droplet on a polymer surface, the largest one is advancing contact angle whereas the smallest one is receding contact angle. The difference between advancing and receding contact angles is called contact angle hysteresis. The contact angle hysteresis could be due to substrate roughness and heterogeneity, impurities on the substrate etc.

The degree that a polymer surface is wetted by a liquid is defined as the wettability of the surface. The wettability of a polymer surface is evaluated by examining the profile of a test liquid droplet which keeps in contact with the polymer, and characterized by contact angle as shown **Figure 2.5**. The wettability of a solid is classified as i) $\theta > \pi/2$ (unwettable), ii) $0 < \theta < \pi/2$ (partially wettable) and iii) $\theta = 0$ (completely wettable). A water wettable surface is known as hydrophilic (or lyophilic) surface, whereas unwettable surface is considered as a hydrophobic (or lyophobic) surface.

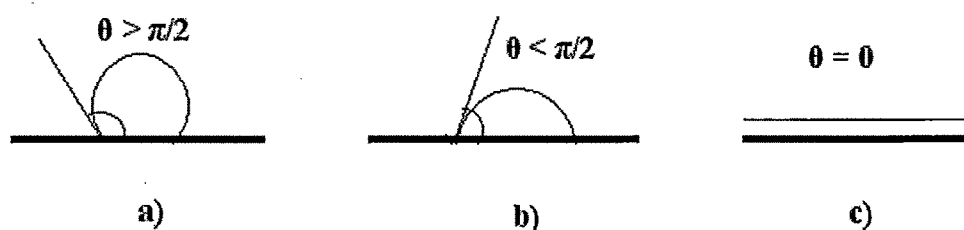


Figure 2.5: a) Non-wetting of solid surface ($\theta > \pi/2$), b) Partial wetting of solid surface ($\theta < \pi/2$) and c) Complete wetting of solid surface ($\theta = 0$)

(b) Estimation of Surface free energy

Molecules at the surface are known to have different properties than the ones in the bulk. This arises from the fact that surface molecules experience different

forces than the bulk molecules and these forces occur as a result of attractions between the neighboring molecules as well as the molecules that exist in the environment. The molecules in the bulk have no net force acting on them while the ones at the surface encounter a net force inwards. This phenomenon results in a tension or free energy at surface which is called 'Surface Tension' or 'Surface Free Energy' (SFE). SFE is defined as the work required to increase the area of a substance by unit amount and it has the units of mN/m or mJ/m² or dynes/cm. [96]

SFE has polar (γ_s^p) and dispersive (γ_s^d) components which give information about the polar or apolar character of the surface. Their summation give the total SFE (γ_s^{Tot}) as shown in following equation

$$\gamma_s^{\text{Tot}} = \gamma_s^p + \gamma_s^d \quad \text{-----} \quad (2.1)$$

When a drop of a liquid is put onto a solid surface, three interfacial tensions liquid-solid γ_{sl} , liquid-vapour γ_{lv} , and solid-vapour γ_{sv} exists. The contact angle θ , is defined by the Young's equation:

$$\gamma_{sv} = \gamma_{sl} + \gamma_{lv} \cos\theta \quad \text{-----} \quad (2.2)$$

The force responsible for spreading a liquid droplet on solid surface can be given by

$$F = \gamma_{sv} - \gamma_{sl} - \pi_e - \gamma_{lv} \cos\theta \quad \text{-----} \quad (2.3)$$

where θ is contact angle, γ_{sv} , γ_{sl} and γ_{lv} are interfacial tensions (free energies) in solid vapor, solid liquid and liquid vapor interfaces respectively, and π_e is the equilibrium pressure of absorbed vapor of the liquid on the solid.

At thermodynamic equilibrium, the energy of the system must be stationary and $F = 0$, due to the balance between all interactions at the surface i.e. liquid droplet comes to rest (small or zero contact angle, θ , between liquid and solid). This gives us famous Young's equation as [97]

$$\gamma_{sv} - \gamma_{sl} - \pi_e = \gamma_{lv} \cos\theta \quad \text{-----} \quad (2.4)$$

Thus the contact angle is defined and decided by the surface and interfacial energies. Unfortunately, only γ_{lv} and θ are liable to direct experimental determination. In order to understand and predict the adhesion of polymers, it is essential that something be known about γ_{sv} and γ_{sl} .

Zisman et al [98] have made a successful approach to this problem. A plot of $\cos \theta$ vs γ_{lv} for homologous series of liquids on a given solid is generally a straight line and introduced a concept of critical surface tension of wetting (γ_c).

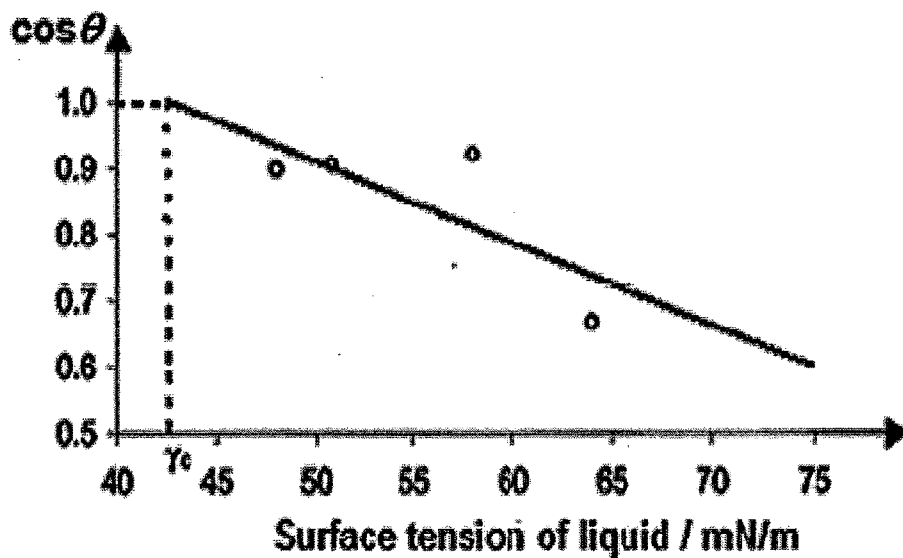


Figure 2.6: Zisman plot for estimating surface tension of liquid

$$\cos \theta = 1 - b(\gamma_{lv} - \gamma_c) \quad \text{-----} \quad (2.5)$$

where b is the slope of the regression line. Extrapolation of this line to the point of $\cos \theta = 1$ yields the value of $\gamma_{lv} = \gamma_c$ at the point. Liquids of γ_{lv} less than γ_c would be expected to spread on the solid surface. [97]

Hence, equation (2.4) implies that

$$\gamma_c = \gamma_{sv} - \gamma_{sl} - \pi_c \quad \text{-----} \quad (2.6)$$

Many researchers have been inclined to identify γ_c and γ_{sv} . Zisman carefully pointed out that γ_c is symbatic with, but not necessarily equal to the solid surface free energy because it is not certain that γ_{sl} and $\pi_c = 0$ when $\theta = 0$.

Fowkes in a theoretical consideration of attractive forces at interfaces has suggested that the total free energy at a surface is the sum of contributions from the different intermolecular forces at the surface. [97] Thus the surface free energy of water could be written as

$$\gamma_{lv} = \gamma_l^d + \gamma_l^h \quad \text{-----} \quad (2.7)$$

where the superscripts h and d refer to the hydrogen bonding and dispersion force components.

By assuming $\pi_c = 0$ and

$$\gamma_{sl} = \gamma_{sv} + \gamma_{lv} - 2 (\gamma_s^d \gamma_l^d)^{1/2} \quad \text{-----} \quad (2.8)$$

Fowke's has derived from the Young equation an expression for the contact angle of a liquid on a solid in terms of the dispersion force contributions of each:

$$1 + \cos \theta = 2 (\gamma_s^d)^{1/2} ((\gamma_l^d)^{1/2} / \gamma_{lv}) \quad \text{-----} \quad (2.9)$$

Since values of γ_l^d have been published for many liquids, it is possible to approximate γ_s^d from a single measurement of θ where only dispersion forces operates (i.e. the liquid or solid is nonpolar).

For cases whether both forces operates, assume that equation (2.8) has more general form

$$\gamma_{sl} = \gamma_{sv} + \gamma_{lv} - 2 (\gamma_s^d \gamma_l^d)^{1/2} - 2 (\gamma_s^h \gamma_l^h)^{1/2} \quad \text{-----} \quad (2.10)$$

Solving equations (2.2) and (2.8), we get

$$\gamma_{lv} (1 + \cos\theta) = 2((\gamma_s^d \gamma_l^d)^{1/2} + (\gamma_s^h \gamma_l^h)^{1/2}) \quad \text{-----} \quad (2.11)$$

The use of equation (2.11) would require dispersive and polar component values of two test liquids' surface tension data whose contact angles on the surface are known or obtained. Solving the equations for the surfaces by simultaneously putting the dispersive and polar component values of liquids' SFE lead to surface's energy components. Using Eq. 2.11, total SFE is the summation of these two components.

2.3.2 Vicker's Microhardness

Microhardness measurement provides information, which can be correlated to wear resistance, ductility, tensile strength and other physical characteristics of the material. The Vickers microhardness measurement is often easier to use than other hardness tests since the required calculations are independent of the size of the indenter, and the indenter can be used for all materials irrespective of hardness. The indent is produced by applying a known load to the specimen and then measuring the size of the appropriate diagonals either optically or with

image analysis software. The Vickers hardness (H_V) number is obtained by dividing the applied load in kilogram-force by the surface area of the indentation. The area of the indentation produced from the Vickers square-based pyramidal diamond is determined by the mean distance between the two diagonals of the indentation. During the experiment smooth and clean surface was subjected to indentation test at room temperature using Vickers microhardness tester (Future Tech. Corp., Japan FM-700) as shown in **Figure 2.7**.



Figure 2.7: *Vicker's Microhardness Indenter Future Tech. (FM-700)*

Principles:

This method was developed by W.C Oliver to measure the hardness of a material from indentation load-displacement data obtained during one cycle of loading and unloading. A schematic representation of a typical data set obtained with a Berkovich indenter (triangular pyramid) is presented in **Figure 2.8**, where the parameter P designates the load and h the displacement relative to the initial undeformed surface. For modeling purposes, deformation during loading

is assumed to be both elastic and plastic in nature as the permanent hardness impression forms. During unloading, it is assumed that only the elastic displacements are recovered; it is the elastic nature of the unloading curve that facilitates the analysis. For this reason, the method does not apply to materials in which plasticity reverses during unloading. [99]

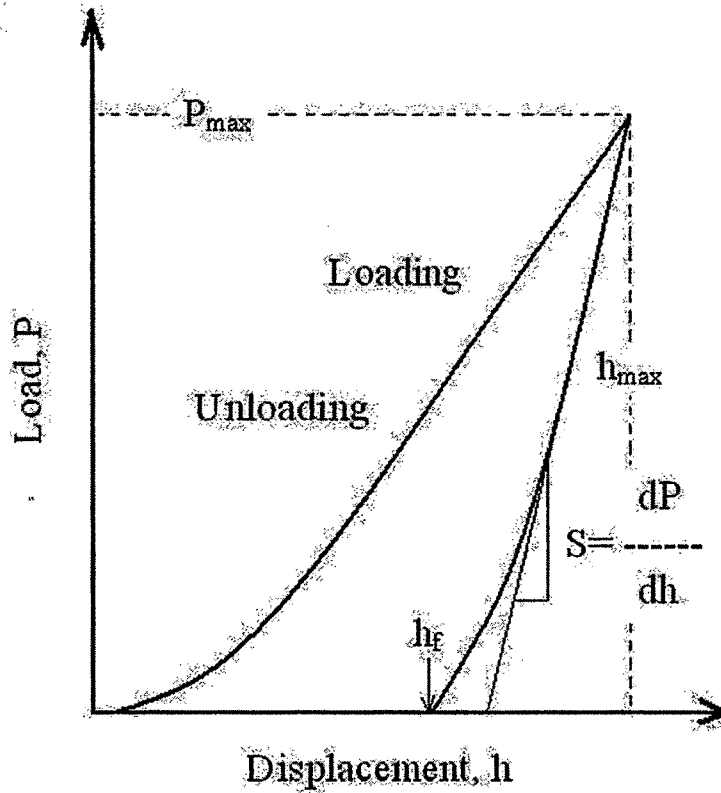


Figure 2.8: Schematic illustration of indentation load-displacement data showing important measured parameters (Ref. 99, 100)

There are three important quantities that must be measured from the P-h curves: the maximum load, P_{\max} , the maximum displacement, h_{\max} , and the elastic unloading stiffness, $S = dP/dh$, defined as the slope of the upper portion of the unloading curve during the initial stages of unloading (also called the contact stiffness). The accuracy of hardness measurement depends inherently on how

well these parameters can be measured experimentally. Another important quantity is the final depth, h_f , the permanent depth of penetration after the indenter is fully unloaded.

The analysis used to determine the hardness, H , is essentially an extension of the method proposed by Doerner and Nix [101] that accounts for the fact that unloading curves are distinctly curved in a manner that cannot be accounted for by the flat punch approximation. In the flat punch approximation used by Doerner and Nix, the contact area remains constant as the indenter is withdrawn, and the resulting unloading curve is linear. In contrast, experiments have shown that unloading curves are distinctly curved and usually well approximated by the power law relation: $P = \alpha(h - h_f)^m$

Where α and m are power law fitting constants. [99, 100]

The variation of the power law exponents in the range $1.2 \leq m \leq 1.6$ demonstrates not only that the flat punch approximation is inadequate ($m = 1$ for the flat punch), but also that the indenter appears to behave more like a paraboloid of revolution, for which $m = 1.5$. [99, 102] This result was somewhat surprising because the axisymmetric equivalent of the Berkovich indenter is a cone, for which $m = 2$.

The exact procedure used to measure H is based on the unloading processes shown schematically in **Figure 2.9**, in which it is assumed that the behavior of the Berkovich indenter can be modeled by a conical indenter with a half-included angle, Φ , that gives the same depth-to-area relationship, $\Phi = 70.3^\circ$. The basic assumption is that the contact periphery sinks in a manner that can be described by models for indentation of a flat elastic half-space by rigid punches of simple geometry.[102] This assumption limits the applicability of the method

because it does not account for the pile-up of material at the contact periphery that occurs in some elastic-plastic materials. Assuming, however, that pile-up is negligible, the elastic models show that the amount of sink-in, h_s , is given by:

$$h_s = \epsilon \frac{P_{\max}}{s} \quad (2.12)$$

Where ϵ is a constant that depends on the geometry of the indenter. Important values are: $\epsilon = 0.72$ for a conical punch, $\epsilon = 0.75$ for a paraboloid of revolution (which approximates to a sphere at small depths), and $\epsilon = 1.00$ for a flat punch. [102] Based on the empirical observation that the unloading curves are best approximated by an indenter that behaves like a paraboloid of revolution ($m = 1.5$), the value $\epsilon = 0.75$ was recommended and has since become the standard value used for analysis.

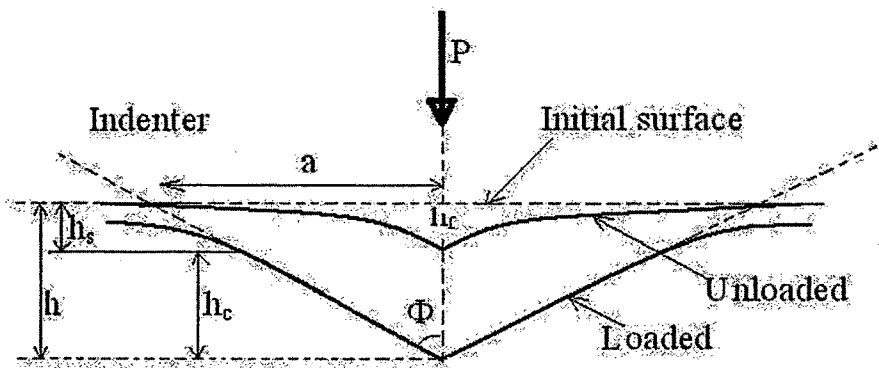


Figure 2.9: Schematic illustration of the unloading process showing parameters characterizing the contact geometry (Ref. 99, 100)

Using Eq. 2.12 to approximate the vertical displacement of the contact periphery, it follows from the geometry of **Figure 2.9** that the depth along which contact is made between the indenter and the specimen, $h_c = h_{\max} - h_s$, is:

$$h_c = h_{\max} - c \frac{P_{\max}}{S} \quad (2.13)$$

Letting $F(d)$ be an “area function” that describes the projected (or cross sectional) area of the indenter at a distance d back from its tip, the contact area A is then

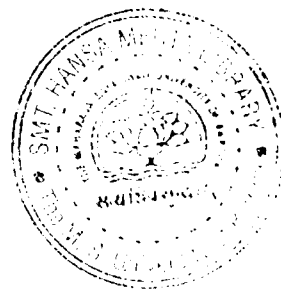
$$A = F(h_c) \quad (2.14)$$

The area function, also sometimes called the indenter shape function, must carefully be calibrated by independent measurements so that deviations from nonideal indenter geometry are taken into account. These deviations can be quite severe near the tip of the Berkovich indenter, where some rounding inevitably occurs during the grinding process. Although a basic procedure for determining the area function was presented as part of the original method, a significant changes have been made to it in recent years.

Once the contact area is determined, the hardness is estimated from:

$$H = \frac{P_{\max}}{A} \quad (2.15)$$

Although it was originally intended for application with sharp, geometrically self-similar indenters like the Berkovich triangular pyramid, we have since realized that it is much more general than this and applies to a variety of axisymmetric indenter geometries including the sphere.



In general, Vickers Hv is computed from,

$$H_v = \frac{2 P \sin(\alpha/2)}{d^2} \quad \text{-----} \quad (2.16)$$

Where P is the indenter load in kilogram-force, d is the average of the two diagonal lengths in millimeters, and α is the face angle of the ideal indenter, which is 136° .

Generally, units of gram-force (gf) and micrometers (μm) are used in this field.

Therefore, Vickers' hardness number, Hv was calculated using the relation

$$H_v = 1854.4 \times P / d^2 \quad (\text{Kgf/mm}^2) \quad \text{-----} \quad (2.17)$$

Where P is the indenter load in gram-force, d is the average of the two diagonal lengths in micrometers.

Procedure:

Digital Microhardness Tester (FM 700 –Future-Tech Corporation, Kawasaki-Japan) shown in **Figure 2.7** was used to determine the Vicker's hardness number (Hv) by the indentation technique. Microhardness measurements on pristine and treated films were carried out by means of Vickers' microhardness tester. Indentation was made with a Vickers' diamond pyramidal indenter housing a square base and pyramidal angle of 136° between the opposite faces attached to an optical microscope using a pillar micrometer/image analyzer. The samples fixed with non-reactive adhesive on an optical glass plate in such a way that the surface to be indented was perfectly horizontal. The plate along with the sample was then mounted on the stage of microscope so as to avoid only displacement of samples during indentation. The load ranging from 10 to 500 gf was applied for a constant loading time of 20 s. The average value of diagonal

of indentation was used for the calculation of hardness value. In the beginning, H_v increases with indentation depth, but as the depth of impression of diamond pyramid increases further, the influence of the distorted zone becomes less significant. This concludes that there is almost no variation of H_v at higher load.

2.3.3 X-ray photoelectron spectroscopy (XPS)

2.3.3.1 The background of XPS

X-ray photoelectron spectroscopy (XPS) involves irradiation of a sample with soft X-rays and the energy analysis of emitted photoelectrons generated from the surface. The X-ray irradiation causes photoionization of atoms in the specimen and the response of the specimen is observed by measuring the energy spectrum of the emitted electrons.

The kinetic energy E_k of the emitted photoelectrons is given by

$$E_k = h\nu - E_b \quad \text{-----} \quad (2.18)$$

Where $h\nu$ is the X-ray energy and E_b is the binding energy of the core electrons of the element

The photoemission and relaxation processes (X-ray fluorescence (XRF) and Auger electron emission (AES)) that occur during X-ray irradiation are shown in **Figure 2.10**. Normally, vacuum level should be chosen as zero level energy, but in XPS and AES binding energies are measured with respect to the Fermi level.

If the core level (for example the K level) is ionized by an incident photon, whose energy $h\nu$ is greater than the binding energy E_b of an electron in the K level, the emitted electron leaves a hole in the core level. If the photoelectrons have sufficient kinetic energy, they are able to escape from the surface by

overcoming the work function Φ_s of the specimen, and photoemission is said to occur.

The kinetic energy E_k at which electrons are emitted is given by:

$$E_k = h\nu - E_b - \Phi_s \quad \text{-----} \quad (2.19)$$

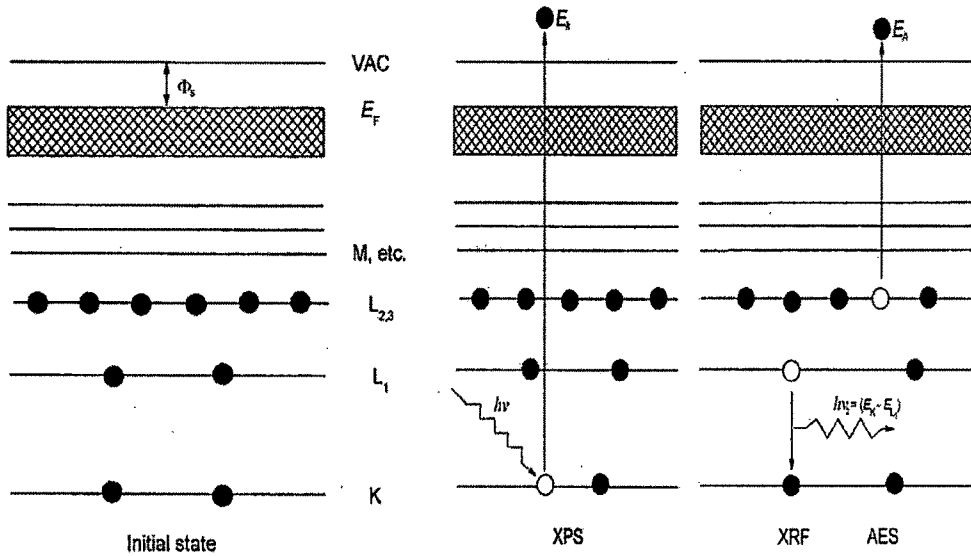


Figure 2.10: Photoemission and subsequent relaxation processes, XRF and AES

Auger series are the result of one of the decay mechanisms of the core-hole created during photoemission. Following the creation of the hole in the K level, the atom relaxes by filling the hole with an electron via transfer (or transition) from an outer level (for example level L_1 as shown in the **Figure 2.10**). The excess kinetic energy $h\nu_2$ becomes available during the transition. This energy is emitted as an X-ray photon, X-ray fluorescence occurs. If the excess energy is transferred to another electron either in the same or in a higher level, emission of an Auger electron with an energy E_A takes place after the electron, e.g. in level $L_{2,3}$, gains the remaining excess energy. After the AES effect took place,

the atom is in a doubly ionized final state. For nearly all elements associated with polymers AES dominates over X-ray fluorescence [103].

In every XPS spectrum, the peaks can be divided into three classes: peaks due to photoemission from core levels, from valence levels, and Auger series due to Auger emission. With Mg K_{α} and Al K_{α} photons at least one core level is excited for any element in the periodic table (except hydrogen) and the characteristic binding energy values allow elemental identification. The core level spectra consist of separate, sharp, clearly identifiable peaks.

Valence levels are those occupied by electrons of low binding energies (0 – 20 eV) which are involved in delocalization or bonding orbitals. Here, the spectrum consists of many closely spaced levels giving rise to a band structure. Auger series result from the decay mechanism for core hole states. Because some of the levels involved can be quite close in energy, there are several competing processes which give rise to a series of peaks in a particular region of the XPS spectrum.

The soft X-rays penetrate many microns deep into the sample. But only surface photoelectrons leave the sample without inelastic collisions retaining their original kinetic energy and so that they contribute to the peaks. Other electrons suffer inelastic collisions resulting in energy loss during the movement through the solid. These losses usually give rise to the step-like increase in the background on the low kinetic energy side of the spectra. The probability of an inelastic scattering event to occur is determined by both the kinetic energy of the electron and the material through which it is travelling. For the photoelectrons emitted with a certain angular distribution from a depth z below the surface, the intensity can be written as:

$$I_z = I_0 \exp (-z/\lambda \sin \theta) \quad \text{-----} \quad (2.20)$$

where I_z is the intensity originating from the atoms at depth z , I_0 is the intensity from the surface atoms and θ is the electron take-off angle with respect to the surface. In this case, λ is the inelastic mean free path of the detected electrons, defined as the average distance that an electron with a given energy travels between successive inelastic collisions. Because values for λ are derived from 'attenuation' experiments, λ is also called attenuation length. The dependence of λ on kinetic energy is expressed as a power relationship $\lambda = E_k^x$, where x lies between 0.5-0.7 for a wide range of materials, for organic materials $x > 1$ [103]. Due to the exponential decay behaviour (Equation 2.17), it is not possible to derive a unique value for the sampling depth d that varies with the take-off angle and it is the basis of angle-resolved XPS. Commonly 3λ (95% detection) is taken to be the 'sampling depth'. The maximum information depth possible to measure is up to 3 – 10 nm [99], which is approximately the same as the ion range of low energy ions (1 – 5 keV) in a polymer substrate [104]. This is the reason, why XPS is such a surface sensitive technique. It is able to perform elemental analysis because no two atoms of the periodic table have the same set of binding energies. Moreover, XPS can be used to collect information on the electronic structure and the chemical environment, since for the same kind of atom the energy levels change with their oxidation states or with their net charge.

2.3.3.2 Instrumentation

A schematic diagram of an XPS instrument (VSW ESCA) used is shown in **Figure 2.11**. The spectrometer consists of a vacuum chamber, an X-ray source,

an electron energy analyzer, a detection system, and a data acquisition system controlled by a PC.

It is necessary to have good vacuum in order for the photoelectrons to reach the analyser without being scattered by residual gas molecules. In our experiment, the vacuum in the analysis chamber is of the order of 1.33×10^{-9} mbar. This ultra-high vacuum condition is enough to avoid electron scattering, and to reduce the contamination (or increase the time for adsorption of a monolayer of contaminants) of the sample surfaces with the residual gas molecules.

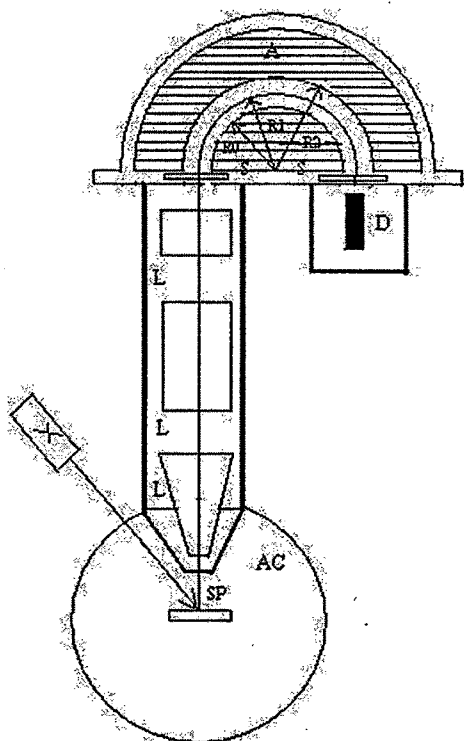


Figure 2.11: Schematic diagram of an XPS instrument. *A* – analyser, *AC* – analysis chamber, *L* – focus and retardation lenses, *D* – detector, *S* – slits, *SP* – specimen, *X* – X-ray source

X-rays are generated in the X-ray source by bombarding an anode with high energy electrons from a heated filament. The emission spectrum consists of characteristic lines, emitted due to electronic transitions of outer shell electrons

into the core-holes created by the impact of the electrons. The X-ray source used in our experiments contains a double anode system featuring aluminium and a magnesium anode, from which K α X-rays having energies of 1486.6 eV for Al, and 1253.6 eV for Mg are emitted. These types of X-rays have sufficient energy to excite core-level electrons of all elements. The characteristic linewidths are relatively narrow (Al 0.85 eV, Mg 0.7 eV) minimizing the contribution to the photoelectron linewidth.

Emitted electrons are collected, retarded and analysed in the analyser in which the energy distribution of the electrons emitted from the sample is measured and the photoelectron spectrum is plotted as intensity versus kinetic energy. The EA 125 concentric hemispherical analyser (CHA), connected to XPS system, is composed of two concentric hemispheres. The inner and outer hemispheres are biased negatively and positively with respect to the pass energy of the analyser. The analyser disperses electrons according to their energy across the exit plane and focuses them in the angular dimension, from the entrance to the exit plane.

The input lens collects the electrons from the source or target and focuses them onto the entrance of the analyser simultaneously adjusting their kinetic energy to match the pass energy of the analyser. The lens is also designed to define the analysed area and angular acceptance of electrons which pass through the hemispherical analyser. The length design employs a double length concept, where the first length selects the spot size and the angular acceptance, while the second lens retards or accelerates the electrons to match the pass energy of the analyser.

The detector consists of a five channel electron multiplier (channeltrons), placed across the exit plane of the analyser, amplify the current of a single electron.

The transmitted electrons are dispersed in energy across the analyser slit by $2R_0/E_p$ mm eV⁻¹ (E_p is the pass energy). The small current pulse present at the output of the channeltron is passed through a vacuum feed through to a preamplifier. From here the signal is passed on to pulse counter for processing and production of an electron energy spectrum. As it was already mentioned above, emitted photoelectrons leave the sample with a kinetic energy given by the Equation 2.19.

The true kinetic energy scale cannot be measured directly because Φ_s varies from sample to sample and it is not known. The offset of the spectrum by Φ_s is not important since the kinetic energy measured with the analyser is important. The ejected electrons pass through the first length element and then are retarded by an amount R , determined by the lens voltages, before entering the analyser. The analyser is a band pass filter only transmitting electrons with an energy very near to the pass energy E_p . Therefore electrons have a measured kinetic energy $E_k = R + E_p$. But the analyser has its own work function Φ_a . Therefore electrons which have been transmitted by the analyser with a retardation of E_p would have a kinetic energy that is independent of the work functions of the sample:

$$E_k = h\nu - E_b - \Phi_a \quad \text{-----} \quad (2.21)$$

2.3.3.3 Polymer surface chemical analysis

In order to understand which chemical changes take place on the polymer surface, the samples were placed in an analytical chamber where XPS analysis was performed after treatment with different gases and different energies and ion fluences. The samples were transferred through the transfer chamber keeping them ion UHV and avoiding exposure to atmosphere.

XPS measurements were performed using an electron spectrometer (Omicron) equipped with a non-monochromated Al K_{α} (1486.6 eV) or Mg K_{α} (1253.6 eV) source. In our experiments, we have used Al K_{α} (1486.6 eV) source. The pass energy was chosen to be 48 eV in order to obtain high resolution elemental spectra of the C1s, O1s and N1s peaks.

The atomic concentration (expressed as at.%) of each element was calculated as follows:

The atomic sensitivity factor (ASF) was used to find the atomic concentration of carbon, oxygen etc. The concentration of carbon in C1s peak and oxygen in O1s peak were determined by dividing its area by atomic sensitivity factor (ASF). [ASF = 0.25 for Carbon (C) and ASF = 0.66 for oxygen (O)]. It is important to use the high magnification X-ray beam because it is important to record the signal from the modified area only. High resolution spectra were analysed and peak fitting performed using the Gaussian/Lorentzian curve fitting programme.

The technique based on variation of the vertical sampling depth with photoelectron take-off angle is known as angle-resolved XPS (ARXPS). The major requirement for surface sensitivity enhancement is that the surface must be flat, as the surface roughness leads to an averaging of electron exit angles and also to shadowing effects such that the surface enhancement becomes impossible. The take-off angles were 0, 15, 30, 45, 60 and 75 degrees. This analysis revealed the polymer modification depth and whether functional groups preferably formed on near the surface or deeper in the polymer.

2.3.4 Atomic Force Microscopy

Binnig in 1986 published the first description of AFM. [105] During the last few decades, AFM has been used increasingly to investigate surface modifications at high resolution. The technique can provide three-dimensional images of the surface. AFM imaging is performed by sensing the force between a very sharp tip and the sample surface (Figure 2.12). [106]

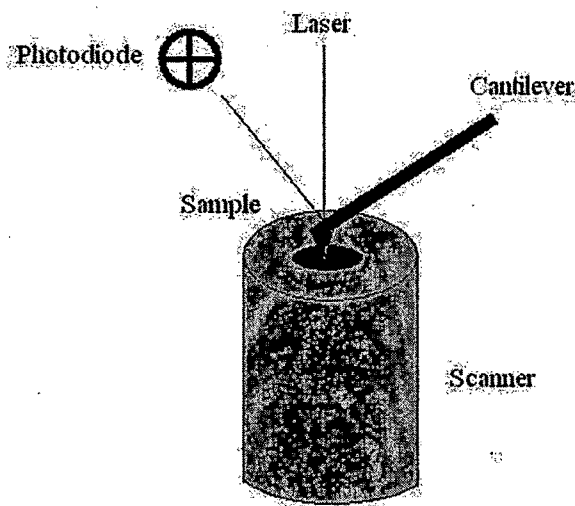


Figure 2.12: *General principle of AFM*

An AFM image is generated by recording the force change as the probe (or sample) is scanned in the x and y direction. The sample is mounted on a piezoelectric scanner, which ensures three-dimensional positioning with high resolution. The force is monitored by attaching the tip to a pliable cantilever and can be measured the bending or “deflection” of the cantilever. The larger cantilever deflection, the higher the force that will be experienced by the probe.[106]

This force can be described using Hooke’s Law:

$$F=-k \cdot x \quad \text{-----} \quad (2.22)$$

F = Force

k = spring constant

x = cantilever deflection

A laser beam is focused on the free end of the cantilever, and the position of the reflected beam is detected by a position-sensitive detector (photodiode). AFM cantilevers and probes are typically made of silicon or silicon nitride by microfabrication techniques.

The most widely employed imaging mode is the contact mode, in which sample topography can be measured in different ways. In the constant height mode, one simply records the cantilever deflection while the sample is scanned horizontally. To prevent sample damage, minimizing large deflections, thus holding the applied force to small values, is necessary. This is achieved in the constant-deflection mode, in which the sample height is adjusted to keep the deflection of the cantilever constant by using a feedback loop. The feedback output is used to display a true "height image". The height image provides quantitative height measurements, allowing accurate measurement of surface roughness, the height of the surface features, or the thickness of biological layers. The deflection image does not reflect true height variation, but since the frequency response is much higher, it is more sensitive to fine surface details than the height signal. AFM was employed to measure the surface roughness of plasma treated polymers.

Measuring the force acting between the AFM tip and the sample, by means of force-distance curves, is important in defining the imaging force and thus in optimizing the image resolution. AFM force measurement can be used to probe the sample's physical properties. Force-distance curves are recorded by

monitoring, at a given x-y location, the cantilever deflection as a function of the vertical displacement of the piezoelectric scanner. A raw curve is a plot of the photodiode voltage versus the scanner position. By using appropriate corrections, this can be converted into a force-versus separation distance curve. The different parts of a force-distance curve can provide a wealth of information. At large probe-sample separation distances, the force experienced by the probe is zero. As the tip approaches the surface, the cantilever may bend upwards due to repulsive forces until it jumps into constant when the gradient of attractive forces exceeds the spring constant plus the gradient of repulsive force. When the probe is retracted from the surface, the curve often shows a hysteresis referred to as the adhesion “pull-off” force, which can be used to estimate the surface energy of solids or the binding forces between complementary molecules.[106, 107]

Modes of Operation:

There are 3 primary imaging modes in AFM:

1. Contact AFM (< 0.5 nm probe-surface separation)

When the spring constant of cantilever is less than surface, the cantilever bends. The force on the tip is repulsive. By maintaining a constant cantilever deflection (using the feedback loops) the force between the probe and the sample remains constant and an image of the surface is obtained.

Advantages: fast scanning, good for rough samples, used in friction analysis

Disadvantages: at time forces can damage/deform soft samples (however imaging in liquids often resolves this issue)

2. Intermittent contact (tapping mode AFM) (0.5-2 nm probe-surface separation)

The imaging is similar to contact. However, in this mode the cantilever is oscillated at its resonant frequency. The probe lightly “taps” on the sample surface during scanning, contacting the surface at the bottom of its swing. By maintaining a constant oscillation amplitude a constant tip-sample interaction is maintained and an image of the surface is obtained.

Advantages: allows high resolution of samples that are easily damaged and/or loosely held to a surface; Good for biological samples

Disadvantages: more challenging to image in liquids, slower scan speeds needed

3. Non-contact AFM (0.1-10 nm probe-surface separation)

The probe does not contact the sample surface, but oscillates above the adsorbed fluid layer on the surface during scanning. Using a feedback loop to monitor changes in the amplitude due to attractive Van der Waals (VdW) forces the surface topography can be measured.

Advantages: VERY low force exerted on the sample (10^{-12} N), extended probe lifetime

Disadvantages: generally lower resolution; contaminant layer on surface can interfere with oscillation; usually need ultra high vacuum (UHV) to have best imaging

The surface morphology of the samples was studied with a Contact mode AFM (Digital Nanoscope IIIa Instrument Inc.) to measure the surface roughness of the plasma treated samples. Root mean square roughness (RMS) was determined as a mean from five scans over the same area.

2.3.5 ATR-FTIR Spectroscopy

ATR-FTIR Spectrometer used to measure the spectra of pristine and all plasma treated polymers. The photograph of the ATR-FTIR spectrometer is shown in **Figure 2.13**.



Figure 2.13: *ATR-FTIR Spectrometer*

2.3.5.1 Principle

Attenuated Total Reflectance (ATR) FTIR is the most widely used FTIR sampling tool. An attenuated total reflection measures the change that occurs in a totally internally reflected infrared beam when the beam comes in contact with the sample as shown in **Figure 2.14**. An infrared beam is directed onto an optically dense crystal with a high refractive index at a certain angle. This internal reflectance creates an evanescent wave that extends beyond the surface of the crystal into the sample held in contact with the crystal. It can be easier to think of this evanescent wave as a bubble of infrared that sits on the surface of the crystal. This evanescent wave protrudes only a few microns ($0.5 - 5 \mu\text{m}$) beyond the crystal surface and into the sample. Consequently, there must be good contact between the sample and the crystal surface. In regions of the infrared spectrum where the sample absorbs energy, the evanescent wave will be attenuated or altered. The attenuated energy from each evanescent wave is

passed back to the IR beam, which then exits the opposite end of the crystal and is passed to the detector in the IR spectrometer. The system then generates an infrared spectrum.

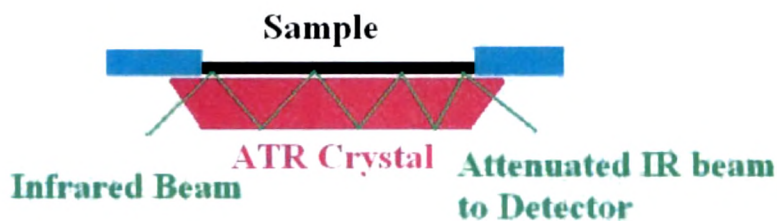


Figure 2.14: *A multiple reflection ATR system*

There are numerous factors that affect the quality of the final spectrum such as

- refractive indices of the ATR crystal and the sample ($n_{\text{crystal}} > n_{\text{sample}}$),
- angle of incident IR beam,
- depth of penetration,
- wavelength of the IR beam,
- number of reflections,
- critical angle
- quality of the sample contact with ATR crystal, etc.

The critical angle (θ_c) is given by

$$\theta_c = \sin^{-1}(n_2/n_1) \quad \text{-----} \quad (2.23)$$

where n_2 is the refractive index of the sample, n_1 is the refractive index of the crystal

When we exceed the critical angle, we will observe a purely ATR spectral result. If the critical angle is not met, we will observe a combined ATR and

external reflectance result. This occurs if the angle of incidence of the IR beam is too low, if the refractive index of the crystal is too low, if the refractive index of the sample is too high or a combination of these 3 factors.

The penetration depth is directly proportional to the wavelength of the incident beam, which means that photons with higher wavenumbers penetrate the sample less than photons with lower wavenumbers. Consequently, peaks on the left hand side often appear a little smaller than expected i.e. OH peaks, etc. It is important to correct this effect by applying the ATR correction to the raw spectrum.

2.3.5.2 Theory

A molecule vibrates, so that the bond lengths between various atoms of the molecule vary periodically. A molecule can have a number of vibrational levels in a given electronic state whose energy is quantized. There can be a number of rotational levels between a pair of vibrational levels. Hence the energy of vibrational transition is larger than energy of a pure rotational transition, but smaller than for an electronic transition. The frequency of vibrational transition lies in the infrared region of the electromagnetic spectrum. The moment infrared radiation are allowed to fall on a molecule, the molecule absorbs the energy, causing the excitation of the molecule to the higher vibrational level.

A molecule with n atoms has $3n$ degrees of freedom. The molecule as a whole can be moved as well as rotated. The translational motion uses 3 degrees of freedom and the rotational motion also uses 3 degrees of freedom. Thus a nonlinear having n atoms has $3n-6$ degrees of freedom. For a linear molecule, there is no rotation about the bond axis and it will have $3n-5$ degrees of freedom. These $3n-6$ or $3n-5$ vibrations are known as normal vibrations or

fundamental vibrations of the molecule. In a molecule, a normal vibration is that in which all the atoms move with the same frequency and are in phase. During a normal vibration, the centre of mass of the molecule remains unchanged. Since a molecule with n atoms has $n-1$ bonds, out of $3n-6$ or $3n-5$ vibrations, $n-1$ would be bond stretching and the rest $2n-5$ or $2n-4$ would be deformation vibrations. [108]

For the vibrations having frequencies ν_1, ν_2, \dots , the energy is

$$E_{\nu_1, \nu_2, \dots} = \sum_i (\nu_i + \frac{1}{2}) h \nu_i \quad \text{-----} \quad (2.24)$$

Where ν_1, ν_2, \dots are vibrational quantum numbers. The corresponding wavenumber is

$$\epsilon_{\nu_1, \nu_2, \dots} = \sum (\nu_i + \frac{1}{2}) \overline{\nu_i} \quad \text{-----} \quad (2.25)$$

where $\overline{\nu_1}, \overline{\nu_2}, \dots$ are wavenumbers for the vibrations. Thus, the zero point energy wavenumber is

$$\epsilon_{0, 0, \dots} = \sum \frac{\overline{\nu_i}}{2} \quad \text{-----} \quad (2.26)$$

Normal vibrations of some simple molecules are discussed in the following.

1) Normal vibrations of CO₂ molecule

The CO₂ is a linear molecule and it has 4 ($= 3 \times 3 - 5$) normal modes. These are shown in **Figure 2.15** and labelled as ν_1, ν_2 and ν_3 . The ν_2 mode actually consists of 2 vibrations; one in the plane of the paper and the other perpendicular to it. Hence it is doubly degenerate. By convention, the modes are labelled in the decreasing frequency within their symmetry type. The first and second modes are symmetric and are known as the symmetric stretching and symmetric bending modes, respectively. These symmetric modes are labelled as ν_1 (highest wavenumber) and ν_2 (next highest). When the molecule is rotated through 180°

about an axis perpendicular to the bond axis and passing through the C atom, these two modes remain unchanged. The asymmetric stretching mode is labelled as ν_3 . The observed values of the vibrational wave numbers are given in brackets.

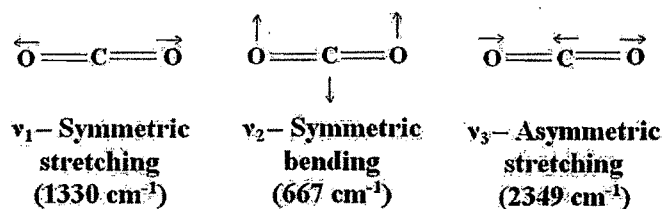


Figure 2.15: Normal modes of CO_2 molecule. The arrows indicate the direction of motion of atoms at a particular instant. Later on the directions are reversed.

2) Normal vibrations of H_2O molecule

The H_2O is a planar molecule having 3 ($= 3 \times 3 - 6$) normal modes shown in **Figure 2.16**. The observed values of the vibrational wave numbers are given in brackets.

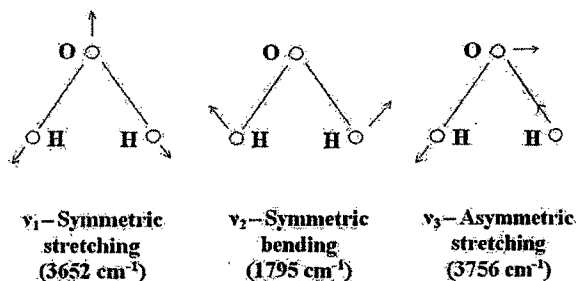


Figure 2.16: Normal modes of H_2O molecule. The arrows indicate the direction of motion of atoms at a particular instant. Later on the directions are reversed.

The stretching frequencies of some of the important bonds in the general absorption regions indicated in following **Table 2.2**.

Bond Type	Absorption Region (cm ⁻¹)
C-C, C-O, C-N	1300 - 800
C=C, C=O, C=N, N=O	1900 - 1500
C≡C, C≡N	2300 - 2000
C-H, O-H, N-H	3800 - 2700

Table 2.2: Some of the important bonds

2.3.5.3 Instrumentation

Attenuated Total Reflection (ATR), is a spectroscopic technique that has the sensitivity to detect very low concentrations of sample near the crystal. In this study, ATR-FTIR is used to study the spectra of chosen samples. A beam of IR light is passed through an ATR crystal, which is usually made from zinc selenide (ZnSe) or germanium. This crystal has the property of being transparent to the IR beam and has a relatively high refractive index. The IR beam is aimed in such a way that it is internally reflected within the crystal at least once. This reflection should take place where the crystal is in contact with the sample of interest for the best results. If this does not occur, the spectroscopic signal of the sample will not be well defined or clean. In the setup used for this study, the beam was bounced about twelve times. This dramatically increases the likelihood that the sample will be in near the crystal in at least one of the places where the beam bounces. The beam reflected by the sample is then collected by a detector once it has exited the crystal. The reflection of the light beam off the internal surface of the crystal forms what is known as an evanescent wave, which penetrates into the sample to a depth of a few micrometers. This phenomenon is used in ATR-FTIR to examine the structure of the sample the wave comes into contact with. After the evanescent wave

interacts with the sample – liquid or solid – it passes back into the crystal and eventually back to the detector, where it is compared with the reference beam. This effect is most efficient when the crystal is made of a material whose optical properties include a refractive index higher than that of the sample. A solid sample is simply pressed into contact with the crystal, and held in place using a clamp or a press to prevent trapped air from distorting the signal. In the case of a liquid sample, there must be a shallow layer over the crystal. This is achieved by injecting the liquid into a flow cell, which creates a thin layer of fluid on the crystal. [109]

Transmission FTIR is done primarily on solid samples, such as polymer films, since it requires the sample to be perpendicular to the beam of IR light, a feat that is difficult to accomplish with a liquid sample. In this method, the IR light beam is passed directly through the sample and to the detector. The amount of light reaching the detector (I) through the sample is compared with the amount of light generated by the IR light source (I_0) to calculate the transmittance of the sample. Transmittance follows the relationship:

$$T = I/I_0 \quad \text{-----} \quad (2.27)$$

The results can be plotted as percent transmittance, though absorbance is most commonly used. Absorbance is calculated using the following relationship:

$$A = -\log T = -\log_{10} (I/I_0) \quad \text{-----} \quad (2.28)$$

In this work, samples of the untreated and plasma treated films were analysed by ATR-FTIR spectroscopy (JASCO FTIR 4100). Samples ($1.0 \times 1.0 \text{ cm}^2$) of the untreated and plasma treated films were pressed against trapezoidal ZnSe

internal reflection elements. Spectra were recorded at a resolution of 4 cm^{-1} between 4000 cm^{-1} and 400 cm^{-1} .